Journal of Materials Chemistry A

Accepted Manuscript

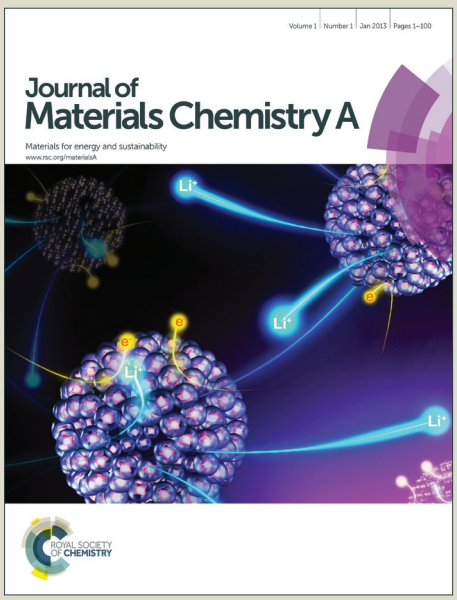

ROYAL SOCIETY OF CHEMISTRY

www.rsc.org/materialsA

Cite this: DOI: 10.1039/c0xx00000x

www.rsc.org/xxxxxx

ARTICLE TYPE

Facile synthesis of $PbTiO_3$ truncated octahedrons via solid state reaction and their application in low-temperature CO oxidation by loading Pt nanoparticles†

Simin Yin[a‡], Yihan Zhu[b‡], Zhaohui Ren[a]*, Chunying Chao[a], Xiang Li[a], Xiao Wei[a], Ge Shen[a] and Gaorong Han[a]*

Received (in XXX, XXX) Xth XXXXXXXXX 20XX, Accepted Xth XXXXXXXXX 20XX
DOI: 10.1039/b000000x

Perovskite $PbTiO_3$ (PTO) nanocrystals with a truncated octahedral morphology have been prepared by a facile solid state reaction. Pt nanoparticles preferentially nucleated on {111} of PTO nanocrystals exhibit a remarkable low-temperature catalytic activity towards CO oxidation from a temperature as low as 30 °C and achieve 100% conversion at ~50 °C.

In the past decade, perovskite oxide nanostructures have attracted enormous attention because of their fascinating size effect and potential applications in ultra high-density data storage, nanogenerators and catalysts.[1-4] With respect to photocatalyst or gas catalyst utilization, it has been proved that the exposed facets of the nanostructures play an important role in achieving improved catalytic performance in many cases from metals, simple oxides to more complex perovskite oxides, which are tightly associated with the exposed facets as well as catalytic metal particle deposition on them.[5-11] For example, an epitaxial growth of Pt {100} on the {100} facets of perovskite $SrTiO_3$ (STO) cuboids was reported recently, which lowers the reaction temperature by 50 °C of propane oxidation compared with the conventional Pt/Al_2O_3 catalyst.[9-11] Therefore, developing a facile approach to synthesizing faceted nanocrysals, especially perovskite oxides, would be both of fundamental and practical interests. Generally, hydrothermal/solvothermal method is widely used to prepare perovskite oxide with different sizes and shapes, which can be modified by the introduction of organic molecules into the reaction system in the cases of $PbTiO_3$(PTO) and $Pb(Zr,Ti)O_3$ (PZT).[12-14] It was shown very recently that the microemulsion structure during a hydrothermal reaction is essential to the shape evolution of perovskite STO nanocrystals.[15] By a self-template growth process, free-standing, single-crystal and single-domain ferroelectric PTO nanoplates were hydrothermally synthesized, growing along the ab plane of the tetragonal perovskite with the {001} facets exposed.[16] Interestingly, PTO nanoplates loaded with Pt nanoparticles (NPs) were demonstrated to show catalytic activity for CO oxidation below 100 °C. Despite of many efforts, achievement of perovskite oxide nanocrystals with well-defined shapes and facets by a simple method remains challenging. Difficulty arises from the relatively complex crystal structure, composition and well-crystallized conditions.[14-16]

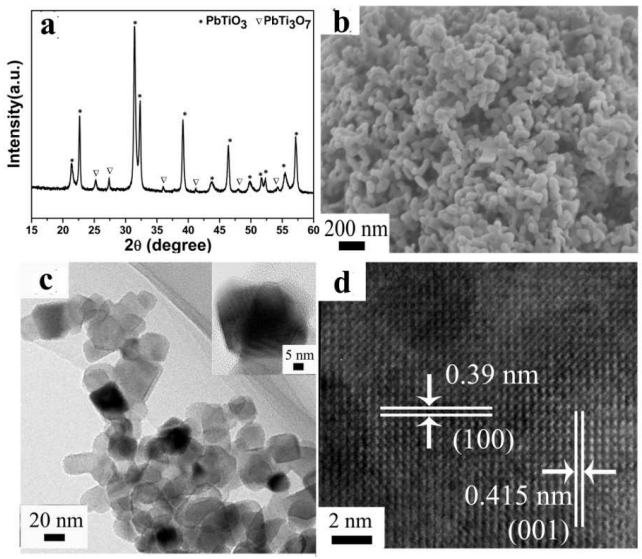

Fig. 1. (a) XRD pattern, (b) SEM image, (c) low-magnification TEM and (d) HRTEM images along [010] zone axis of the as-prepared PTO nanocrystals. Inset in (c) shows high magnitude TEM image of the nanocrystals.

Compared to the hydrothermal/solvothermal method, a solid state reaction usually results in large size and irregularly aggregated particles via a diffusion mechanism, and thus it has scarcely been considered to prepare faceted nanocrystals. Herein, we report a large-scale synthesis of perovskite PTO nanocrystals by a solid state reaction (SSR). Combined with electron tomography and crystallography, it is very interesting to find that these PTO nanocrystals possess a truncated octahedral morphology along the <001> direction, which has rarely been obtained by using a hydrothermal/solvothermal method before. Moreover, Pt NPs has been revealed to preferentially nucleate on the {111} facets of PTO nanocrystals. Such nanocrystals loaded with Pt NPs exhibit remarkable low-temperature catalytic activity towards CO oxidation from a temperature as low as 30 °C and achieve 100% CO conversion at ~50 °C, which makes the Pt/PTO

nanocrystals attractive for possible application in catalytic reaction of NO_x.[17] The catalytic performance present here was discussed on the basis of microstructure analysis.

Single-crystal and single-domain PTO nanoplates have been synthesized by a simple hydrothermal method using TiO_2 (commercial P25) and $Pb(NO_3)_2$ as raw materials.[16] (Preparation, characterization and catalytic experimental details see electronic supplementary information, ESI). When the reaction time is 0.5 h, the obtained sample consists of nanoparticles and thin plates (~20 nm), mainly corresponding to brookite TiO_2 and Pb_3O_4, respectively. When such precursors were heating treated in air at 650 °C for different time, Pb_3O_4 gradually decreased, resulting in the dominated perovskite PTO nanocrystals after 30 min (Fig.S1 and Fig. S2). After 1h, Pb_3O_4 plates completely disappeared, and the sample was characterized in detailed. As shown in Fig. 1a, all the main reflections can be well indexed to a tetragonal perovskite structure (JCPDS: 70-0746), with few weak peaks of $PbTi_3O_7$ (JCPDS: 45-0533) impurity. The as-prepared perovskite PTO has a tetragonality of about c/a=1.06. SEM image (Fig. 1b) shows that the treated sample consists of nanoparticles with an average size distribution of 20~50 nm, confirmed by the TEM image shown in Fig. 1c. HRTEM image along [010] axis in Fig. 1d shows lattice fringes with inter-planar spacing of 0.390 nm and 0.415 nm, corresponding to the tetragonal (100) and (001) plane of perovskite PTO, respectively. Such single-crystal PTO nanocrystals have a Brunauer-Emmett-Teller (BET) external surface area of 14.50 m^2/g, derived from nitrogen adsorption isotherm measured at 77 K (Fig. S3). TG-DSC analysis (Fig. S4) indicates a phase transformation from ferroelectric to paraelectric one occurring at ~491 °C, almost the same to the counterpart of the bulk material.[18] In addition, the exothermal peak at ~289 °C might arise from -OH desorption from the surface of the nanocrystal,[19] matching well with a broad hydroxyl (-OH) stretching peak situated at ~3430 cm^{-1} in the FT-IR spectrum of the sample (Fig. S5).

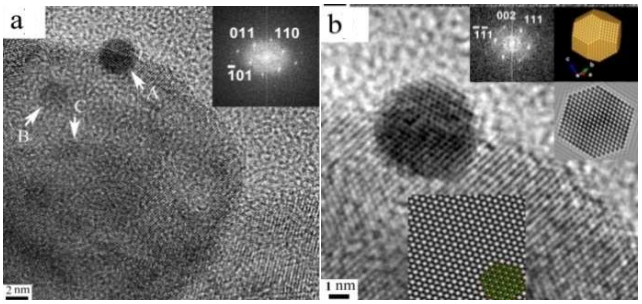

Fig. 2. HRTEM images of (a) Pt/PTO nanocrystal, inset refers to FFT pattern of the PTO nanocrystal and (b) atom-resolved and simulated , upper insets refer to FFT, atomic model and simulated images (Scherzer defocus) of a truncated Pt octahedral along [$1\bar{1}0$] axis. Bottom insets refers to model embedded simulated image (Δf = -90 nm) of PTO nanocrystal along [$1\bar{1}1$] axis. Arrows refer to regions where EDX spectra in Fig. S6 were taken. TEM simulation conditions (Cs =1.2 mm, θ = 1.0 mrad, ΔE = 0.7 eV and 300 kV).

Since the size of PTO nanocrystals is much smaller than that of the nanoplates, we also attempt to evaluate their activity in the catalytic CO oxidation when loaded with Pt NPs. 1.0 wt% Pt NPs with sizes of 3~5 nm were loaded on PTO nanocrystals by a simple wet chemical method (Fig. S7). Before catalytic experiment, the microstructure of Pt/PTO was comprehensively investigated. HRTEM image (Fig. 2a) along the [$1\bar{1}1$] zone axis of PTO nanocrystal explicitly shows the presence of Pt NPs, where the electron beam is perpendicular to the {111} facets of PTO.[20] The HRTEM image and FFT patterns (Fig. 2b) along the [$1\bar{1}1$] zone axis of PTO and [$1\bar{1}0$] zone axis of loaded Pt NP confirm that the Pt NP is single crystal and TEM simulation suggests that its morphology is actually close to truncated octahedron where {111} and {002} facets are exposed. From Fig. 2, Pt NPs is absorbed on the {111} facet of PTO nanocrystals. When prepared by a simple solution reduction reaction without any surface surfactant, {111} facets of Pt NPs tended to expose more easily than other facets such as {100} considering the surface free energy of {111} and {100}(γPt{111}/γPt{100} of 0.84).[21,22]

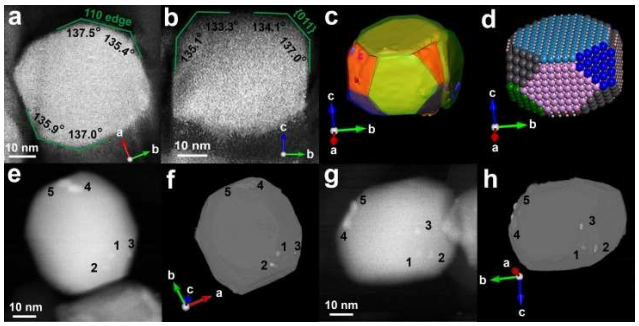

Fig. 3. (a) (001) and (b) (100) slices and (c) volume reconstructed by STEM tomography. Green, orange / blue facets refer to {100}, {111} facets. (d) Atomic model of truncated octahedral PTO nanocrystal. Pink and light blue facets refer to {001} and {100} facets, while grey, blue and green facets refer to {111} facets. (e), (g) two orientations of Pt/PTO nanocrystal and (f), (h) corresponding volumes.

TEM images only provide projected two-dimensional structural information, and unambiguous determination of the morphology of PTO and the nucleation sites of Pt NPs require three-dimensional structural elucidations, which can be achieved by electron tomography. From the reconstructed volume of a ~50 nm PTO nanocrystal by -65°~65° tilt series with a 1° interval as shown in Fig. 3c and Movie S1, together with the previous structural analysis by HRTEM, it is clear that the PTO nanocrystal also has a truncated octahedral morphology with an aspect ratio of ~0.8 along the <001> direction. Based on the (001) and (100) slices of the volume as shown in Fig. 3a and b, both of which have octagon shapes with each interior angle close to 135°, it can be concluded that the nanocrystal is enclosed by {100}, {111} and a small fraction of {011} facets as schematically demonstrated by in Fig. 3d. Comparing the volume and STEM images in Fig. 3e~h, five differently numbered Pt NPs with brighter STEM contrast are found to only nucleates on {111} and {010} facets, the former of which has a perpendicular component of polarization. Moreover, it was discovered that the multiple Pt NPs preferentially nucleated on the {111} facets and a single side of the orthogonal to the polarization direction, where faceted images of PTO namocrystal matched well with a truncated octahedral morphology (Fig. S8).

The above results confirm that the single-crystal truncated octahedral PTO nanocrystals with size of 20~50 nm have been prepared by SSR, where Pt NPs were determined to preferentially nucleate and growth on the {111} facets of PTO nanocrystals. To understand these configurations, the formation of the faceted

PTO nanocrystals is firstly discussed. According to the PbO-TiO_2 phase system, the lowest temperature for the coexistence of liquid phase and cubic perovskite PTO phase is 1111 K.[23] Completely liquid-assisted growth of PTO crystal is not favoured thermodynamically at a temperature of 923 K. Nevertheless, the formation of perovskite phase PTO by SSR is still allowed at this temperature by Ti^{4+} diffusion across PbO, possibly driven by an interface Ti^{4+} gradient.[24] In stark contrast, the bond strength between Ti^{4+} and O^{2-} ions is much higher (~307 kJ/mol) than that between Pb^{2+} and O^{2-} ions (~152 kJ/mol) and the flux of Ti^{4+} ions is relatively negligible.[25,26] In the present work, the product changed significantly from the coexistence of plates and nanoparticles (Pb_3O_4 and TiO_2) to the faceted PTO nanocrystals (Fig.S1 and Fig. 1), which can hardly be explained by a simple diffusion process.[27] It is argued that the melting of the reactants such as Pb_3O_4 nanoplates (a melting point of 773 K for corresponding bulk) may provide a local liquid environment for the nucleation and growth of perovskite PTO. Due to 25 mol% excess of Pb precursor as designed, TiO_2-releated phase completely disappeared, giving rise to a coexistence of lead oxide and PTO phase after a reaction of 10 min at 923 K (Fig. S2). One may expect that TiO_2 nanoparticles were dissolved into melting environment of Pb_3O_4 and quickly exhausted to promote large-scale nucleation and growth of the product, leading to single-crystal PTO nanocrystals with relatively uniform size and well-defined shape. Such SSR process is highly similar to a hydrothermal method, where the excess of Pb precursor is critical to control the size of pre-perovskite PTO nanofibers.[28]

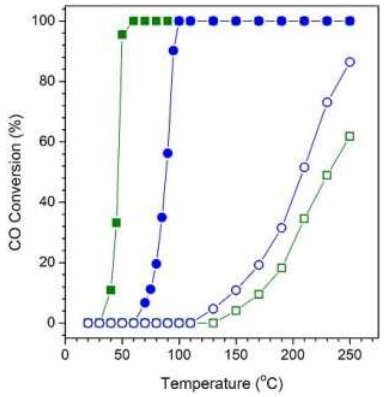

Fig. 4. Catalytic activity of the Pt-loaded (solid) and Pt-free (open) PTO nanocrystals (square) and nanoplates (circle, derived from Ref.16).

For perovskite STO, nearly perfect alignment of Pt{100} (0.392 nm) and STO{100} (0.390 nm) lattice fringes, leading to a strong epitaxy, has been clearly confirmed.[10] By lowering interfacial energy via lattice matching, preferential nucleation and growth of Pt NPs on the {111} facets of PTO nanocrystals are also suggested to be thermodynamically favored. As discussed by first-principle calculations, compared to {001} facets in perovskite PTO, its {111} facets consist of alternating planes of Ti and PbO_3 units, where charges from +4 to -4 developed, resulting in a microscopic electric field.[29] Surface absorptions such as -OH group or reconstrcucted non-stoichiometric terminations are usually expected to compensate such charges. This implies that {111} facets of tetragonal perovskite PTO are not stable thermodynamically. Accoring to the result in Fig.2b, Pt NPs are polyhedron with {111} and {002} facets exposed, allowing us to condiser a possible lattice match occuring between Pt NPs and {111} facets of PTO nanocrystals. Because Pt NPs adopt cubic crystal structure (JCPDS: 04-0802), the lattice spacing of (110) is ~0.277 nm within {111} facets, matching very well with the conuterpart of (110) (~0.276 nm, JCPDS: 70-0746) within {111} facets of tetragonal perovskite PTO (Fig.2a). Therefore, it is argued that the relatively high surface energy of the perovskite PTO {111} facets and the very small lattice mismatch (~0.36%) together contributed to the nucleation and growth of Pt NPs on {111} of tetragonal perovskite PTO nanocrystals, lowering the overall system energy of Pt/PTO. But direct TEM observation of such matched interface is difficult because both of Pt NPs and PTO nanocrystals are complex polyhedron in the present work. Nevertheless, very large lattice mismatch (~29%) between Pt {111} and PTO {001} (~0.390 nm, lattice spacing of (100)), would significantly increase the interfical energy and thus selective nulceation of Pt NPs on the {001} of truncated octahedra PTO are rarely observed. It has been identified that by the similar solution reaction, Pt NPs tended to aggregate with a size of several tens nanometers on {001} of PTO nanoplates[16] (Fig. S9).

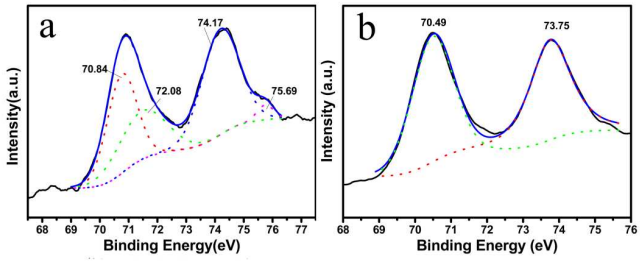

Fig. 5. XPS spectra for Pt 4f of (a) Pt/PTO nanocrystals and (b) Pt/PTO nanoplates

Such structures were then used as a catalyst in CO oxidation. Fig. 4 shows the results of catalytic activity for (Pt-loaded) PTO. It is clear that a low-temperature activity of CO oxidation is triggered by the loading of Pt NPs. Pure PTO supports only have high-temperature activity, which begins at ~150 °C and ends up to 250 °C (Fig. 4). In stark contrast, nearly 100% conversion of CO can be achieved for Pt/PTO nanocrystals at a temperature as low as ~50 °C, which is significantly lower than the temperature of 100% CO conversion (100 °C) for the Pt/PTO nanoplates[16], as shown in Fig. 4. It should be noted that the full CO conversion temperatures for Pt/PTO nanocrystals and nanoplates are much lower than that for the Pt/TiO_2 (~280 °C), Pt/α-Al_2O_3 (~360 °C) and Pt/CeO_2 (~144 °C)[30] and are comparable to the highly active Pt/$H_2Ti_3O_7$ nanotubes (~45 °C)[31]. Although Pt/PTO nanocrystals demonstrate remarkable catalytic performance of CO oxidation at near room temperature, the mechanism involved in it is very complex. We attempt to explain the catalytic activity present here on the basis of a comparison with Pt/PTO nanoplates. It is reasonable to presume that small lattice mismatch is critical for achievement of stable Pt/PTO catalytic structure. Moreover, quick nucleation and growth of Pt due to the small lattice mismatch may also give rise to good dispersion of Pt NPs with a small size via a redox-reduction reaction from H_2PtCl_6 to metallic Pt. Being loaded on PTO nanocrystal and enclosed by {111} and {002} facets, the faceted Pt NPs grew to a size of 3~5 nm on

PTO nanocrystals, whereas Pt NPs tended to form serious aggregation with a size of several tens nanometres on PTO {001} nanoplates[16] (Fig. S9). As a result, the smaller size and more exposed facets of Pt NPs on PTO nanocrystals could provide more active sites for CO oxidation and thus catalytic temperature significantly decreased.

As the size decreased, the ratio of surface oxidized state Pt for Pt nanocubes has been determined to increase gradually, and the counterpart of 5 nm Pt nanopolyhedra is 16.7%.[22] In addition, surface oxidization of metallic Pt at surface and strong Pt-O bonds at interface appear to be prevailed when STO supports are used.[10,11,32,33] XPS analysis on the Pt/PTO nanocrystals and nanoplates was carried out to investigate the chemical states of the surface atoms, as shown in Fig.5. After Gaussian fitting, the binding energies of $Pt4f_{7/2}$ and $Pt4f_{5/2}$ of Pt/PTO nanocrystals are centred at about 70.84 eV, 74.17 eV in Fig.5a, and for Pt/PTO nanoplates, the corresponding values are 70.49 eV and 73.75 eV, shown in Fig.5b. These values indicate the dominant existence of Pt^0 on both of PTO nanocrystals and nanoplates.[34] However, from the nanoplate to the nanocrystal support, the increased binding energies of 0.35 eV and 0.42 eV for $Pt4f_{7/2}$ and $Pt4f_{5/2}$, respectively, imply increased oxidization states of Pt on the PTO nanocrystal. Note that an obvious shoulder of Pt4f5/2 in Fig.5a existing at 75.69 eV is indicative of Pt^{2+} [29] that could be originated from surface oxidation states of Pt NPs, and the ratio of Pt^{2+} was determined to be ~10% by fitting the peak of $Pt4f_{5/2}$. As a comparison, the oxidization states should have made a pronounced contribution to the shoulder in Fig.5a. Nevertheless, Pt^{2+} partially contributed from the interface bewteen Pt and PTO nanocrystals cannot be excluded completely. The formation of Pt-O bonds bewteen Pt and oxide supports was demonstrated to achieve the stable Pt-oxide structures, and a catalyst consisting of metal and metal oxide exhibits an even higher catalytic activity at low temperature.[10,11,31]

On the other hand, the binding energy of Ti2p changes obviously from the nanocrystals to the nanoplates, as depicted in Fig.S10a and b. In the case of Pt/PTO, the binding energy of Ti2p is 458.16eV, indicative of the typical Ti^{4+} ions.[35] For Pt/PTO nanoplates, the binding energy of Ti2p is a mixture contribution of Ti^{3+} (457.1 eV) and Ti^{4+} (458.16 eV). These results lead us to expect that accompained with Ti^{3+}, more defects, such as oxygen vacancies, possibly exist on the surface of PTO {001} nanoplates, which could account for the higher catalytic activity of the Pt-free nanoplates than that of Pt-free nanocrystals in Fig. 4. It also soundly supports that the remarkble catalytic performance of Pt/PTO nanocrystals should be dominantly attributed to the active centres of the loaded Pt NPs, as discussed above. Due to complexity of PTO {111}, a more comprehensive work is desired to elucicate the intercation between Pt NPs and the support as well as its role in the near room-temperature catalytic activtiy for CO oxidation.

In summary, truncated octahedral PTO nanocrystals have been synthesized by a facile solid state reaction (SSR). As a result, Pt nanoparticles (NPs) were revealed to preferentially nucleate and grow on {111} of these PTO nanocrystals, which could be understood by the fact that the small lattice mismatch between Pt {111} and PTO {111} could lead to significant lowering of the interfacial energy and thus a stable Pt/PTO system. Moreover, such system exhibits catalytic activity for CO oxidation from a temperature as low as 30 ^{o}C and achieve 100% CO conversion at ~50 ^{o}C, a 50 ^{o}C lower than that of Pt/PTO {001} nanoplates. Stable Pt/PTO structure, decreased size and formation of surface oxidized states of Pt NPs could be attributed to the observed low-temperature catalytic activity. The findings present here suggest that the shape of perovskite nanostructure as well as its role in guiding nucleation and growth of Pt NPs is of particular importance to optimize catalytic performance.

This work was financially supported by the National Natural Science Foundation of China (No.51232006, 51102212 and 51102208) and Program for Innovative Research Team in University of Ministry of Education of China (IRT13037). We thank the advanced nanofabrication, imaging and characterization core lab of KAUST for support.

Notes and references

[a] *State key Laboratory of Silicon Materials, Department of Materials Science and Engineering, Cyrus Tang Center for Sensor Materials and Applications, Zhejiang University, Hangzhou 310027, P.R. China renzh@zju.edu.cn and hgr@zju.edu.cn*

[b] *Advanced Membranes and Porous Materials Center, King Abdullah University of Science and Technology, Thuwal 23955-6900, Kingdom of Saudi Arabia*

† Electronic Supplementary Information (ESI) available: [details of preparation, characterization and catalytic experiments]. See DOI: 10.1039/b000000x/

‡ These authors contributed equally.

1 X. H. Zhu, Z. G. Liu and N. B. Ming, *J. Mater. Chem.,* 2010, **20**, 4015.

2 N. Nuraje and K. Su, *Nanoscale*, 2013, **5**, 8752.

3 F. Zou, Z. Jiang, X. Q. Qin, Y. X.Zhao, L. Y. Jiang, J. F. Zhi,T. C. Xiao and P. P. Edwards, *Chem. Commun.,* 2012, **48**, 8514.

4 Kato, H.; Sasaki, Y.; Shirakura, N.; Kudo, A. *J. Mater. Chem. A,* 2013, **1**, 12327.

5 Y. N. Xia, Y. J. Xiong, B. Lim and S. E. Skrabalak, *Angew. Chem. Int. Ed.,* 2008, **48**, 60.

6 H. G. Yang, C. H. Sun, S. Z. Qiao, J. Zou, G. Liu, S. C. Smith, H. M.Cheng and G. Q. Lu, *Nature*, 2008, **453**, 638.

7 R. G. Li, F. X. Zhang, D. E.Wang, J. X. Yang, M. R. Li,, J. Zhu, X. Zhou, H. X. Han, and C. Li, *Nat. Comm.*, 2013, **4**, doi: 10.1038/ncomms2401.

8 X. H. Guo, C. C. Mao, J. Zhang, J. Huang, W. N.Wang, Y. H. Deng, Y. Y. Wang, Y. Cao, W. X. Huang and S. H. Yu, *Small,* 2012, **8**, 1515.

9 F. A. Rabuffetti, H.-S. Kim, J. A. Enterkin, Y. M. Wang, C. H. Lanier, L.D. Marks, K. R. Poeppelmeier and P. C. Stair, *Chem. Mater.,* 2008, **20**, 5628.

10 J. A. Enterkin, K. R. Poeppelmeier and L. D. Marks, *Nano Lett.*, 2011, **11**, 993.

11 J. A. Enterkin, W. Setthapun, J. W. Elam, S. T. Christensen, F. A. Rabuffetti, L. D. Marks, P. C. Stair, K. R. Poeppelmeier and C. L. Marshall, *ACS Catal.,* 2011, **1**, 629.

12 G. Xu, Z. H. Ren, P. Y. Du, W. J. Weng, G. Shen and G. R. Han, *Adv. Mater.*, 2005, **17**, 907.

13 G. Z. Wang, R. Sæterli, P. M. Rørvik, A. T. J. V. Helvoort, R. Holmestad, T. Grande and M.-A. Einarsrud, *Chem. Mater.,* 2007, **19**, 2213.

14 Z. H. Ren, G. Xu, X. Wei, Y. Liu, G. Shen and G. R. Han, *J. Am. Ceram. Soc.,* 2007, **90**, 2645.

15 L. H. Hu, C. D. Wang, S. Lee, R. E. Winans, L. D. Marks and K. R. Poeppelmeier, *Chem. Mater.,* 2013, **25**, 378.

16 C. Y. Chao, Z. H. Ren, Y. H. Zhu, Z. Xiao, Z. Y. Liu, G. Xu, J. Q. Mai, X. Li, G. Shen and G. R. Han, *Angew. Chem. Int. Ed.,* 2012, **124**, 9283.

17 A. M. Kolpak, I. Grinberg and A. M. Rappe, *Phys. Rev. Lett.*, 2007, **98**, 166101.

18 A. M. Glazer and S. A. Mabud, *Acta Cryst. B* 1978, **34**, 1065-1067.

19 M. Traianidis, C. Courtois and A. Leriche, *J. Eur. Ceram. Soc.,* 2000, **20**, 2713.

20 Y. F. Hao, G. W. Meng, C. H.Ye and L. D. Zhang, *Cryst. Grow. Design,* 2005, **5**, 1617.

21 L. Vitos, A. V. Ruban, H. L. Skriver and J. Kollar, *Surf. Sci.,* 1998, **411** (1-2), 186.

22 C.-K. Tsung, J. N. Kuhn, W.Y. Huang, C. Aliaga, L.-I. Hung, G. A. Somorjai and P. D.Yang, *J. Am. Chem. Soc.,* 2009, **131**, 5816.

23 B. Jaffe, *Piezoeletric Ceramics*, Academic Press (In Chinese), 1971, P.118.

24 S. S. Chandratreya, R. Fulrath and M. J. A. Pask, *J. Am. Ceram. Soc.*, 1981, **64**, 422.

25 W.D. Kingery, H. K. Bowen and D. R. Uhlmann, *Introduction to Ceramics,* 2nd ed. John Wiley & Sons, New York, 1976, P. 99.

26 Y.-M. Sung, W.-C.Kwak and S. Kim, *J. Mater. Res.,* 2002,**17**, 407.

27 V. I. Levitas, Z. H. Ren, Y. W. Zeng, Z. Zhang and G. R. Han, *Phys. Rev. B,* 2012, **85**, 220104(R).

28 Z. Y. Liu, Z. H. Ren, Z. Xiao, C. Y. Chao, X. Wei, Y. Liu, X. Li, G. Xu, G. Shen and G. R. Han, *Small,* 2012, **8**, 2959.

29 Q. Pang, J. M. Zhang, K. W. Xu and V. Ji, *Appl. Surf. Sci.*, 2009, **255** , 8145.

30 H. P. Zhou, H. S.Wu, J. Shen, A. X.Yin, L. D. Sun and C. H. Yan, *J. Am. Chem. Soc.*, 2010, **132**, 4998.

31 A. V. Grigorieva, E. A. Goodilin, L. E. Derlyukova, T. A. Anufriev, A. B. Tarasov, Y. A. Dobrovolskii and Y. D. Tretyakov, *Appl. Catal. A-Gen.,* 2009, **362**, 20.

32 A. D. Polli, T. Wagner, T. Gemming and M. Rühle, *Surf. Sci.* 2000, 448, 279-289.

33 A. Asthagiri and D. S. Sholl, *J. Chem. Phys.,* 2002,**116**, 9914.

34 C. D. Huang, K. S.Tan, J.Y. Lin and K. L. Tan, *Chem. Phys. Lett.,* 2003, **371**, 80.

35 Moulder, J.; Stickle, W.; Sobol, F. P. E. K.; Bomben, D. *Handbook of X-ray photoelectron spectroscopy*. Perkin Elmer Corporation, Physical Electronics 1992, P.73.